Electronic Supplementary Material (ESI) for CrystEngComm.
This journal is © The Royal Society of Chemistry 2019

Supplementary information

A Bifunctional 3D Tb-based Metal−Organic Framework for Sensing and Removal of Antibiotics in Aqueous Medium

Jie Zhang,[a] Lingling Gao,[a] Yang Wang,[a] Lijun, Zhai,[a] Xiaoyan Niu,[a] and Tuoping Hu*[a]

Table. S1 Selected bond lengths/Å and bond angles/º for complex (**1**).

Complex **1**					
Tb1-O1	2.408(2)	Tb1-O2^{1}	2.380(2)	Tb1-O6^{3}	2.364(2)
Tb1-O1^{1}	2.668(2)	Tb1-O5^{2}	2.327(2)	Tb1-O8^{4}	2.252(2)
Tb1-O9^{5}	2.303(2)	Tb1-O10	2.434(2)		
O1-Tb1-Tb1^{1}	40.84(5)	O5^{2}-Tb1-O2^{1}	83.69(8)	O6^{3}-Tb1-O2^{1}	96.17(9)
O1-Tb1-O1^{1}	77.02(7)	O5^{2}-Tb1-O6^{3}	136.35(8)	O6^{3}-Tb1-O10	151.09(8)
O1-Tb1-O10	133.03(8)	O5^{2}-Tb1-O10	71.51(8)	O6^{3}-Tb1-C1^{1}	85.49(9)
O2^{1}-Tb1-O1	127.69(7)	O6^{3}-Tb1-O1^{1}	75.53(8)	O8^{4}-Tb1-Tb1^{1}	122.87(5)
O2^{1}-Tb1-O1^{1}	51.01(7)	O6^{3}-Tb1-O1	73.27(7)	O8^{4}-Tb1-O1	82.15(7)
O2^{1}-Tb1-O10	76.92(9)	O8^{4}-Tb1-O10	74.65(9)	O8^{4}-Tb1-O1^{1}	158.77(7)
O5^{2}-Tb1-O1	72.76(8)	O9^{5}-Tb1-O1^{1}	116.02(7)	O8^{4}-Tb1-O2^{1}	148.72(8)
O5^{2}-Tb1-O1^{1}	70.78(7)	O9^{5}-Tb1-O1	141.21(8)	O9^{5}-Tb1-O5^{2}	145.25(8)
O8^{4}-Tb1-O5^{2}	99.27(8)	O9^{5}-Tb1-O2^{1}	77.58(8)	O9^{5}-Tb1-O6^{3}	75.25(8)
O8^{4}-Tb1-O6^{3}	102.40(8)	O10-Tb1-Tb1^{1}	136.25(6)	O9^{5}-Tb1-O10	75.85(9)
O8^{4}-Tb1-O9^{5}	83.06(7)	O10-Tb1-O1^{1}	117.41(8)		

Symmetry codes: ^{A}-X,-Y,-Z;^{B}1-X,-1+Y,1/2-Z;^{C}-1+X,1-Y,-1/2+Z;^{D}+X,-1+Y,+Z;^{E}-X,-1+Y,1/2-Z.

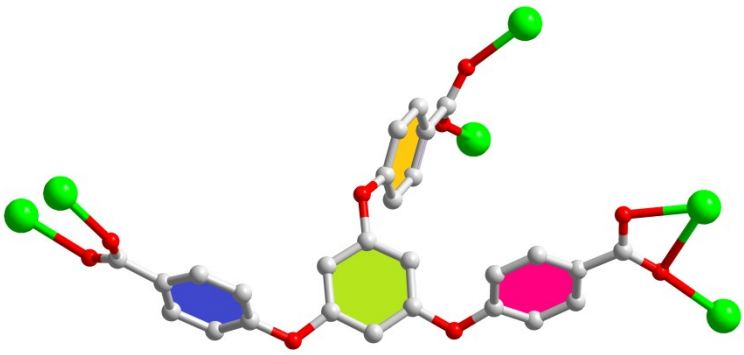

Fig.S1 The coordinated mode of Tb-MOF.

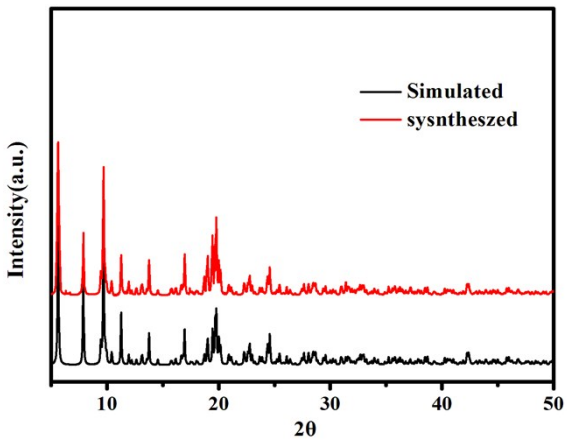

Fig. S2. PXRD patterns of Tb-MOF.

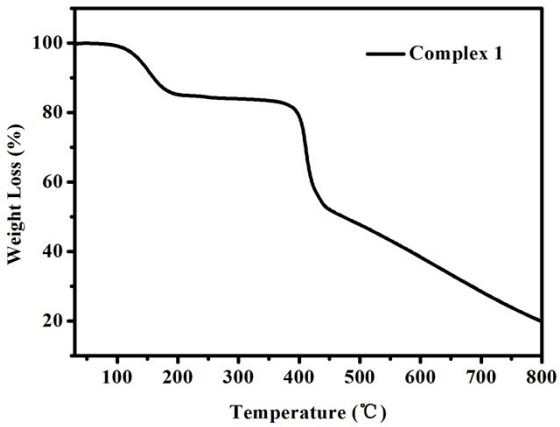

Fig. S3. TG curve of Tb-MOF.

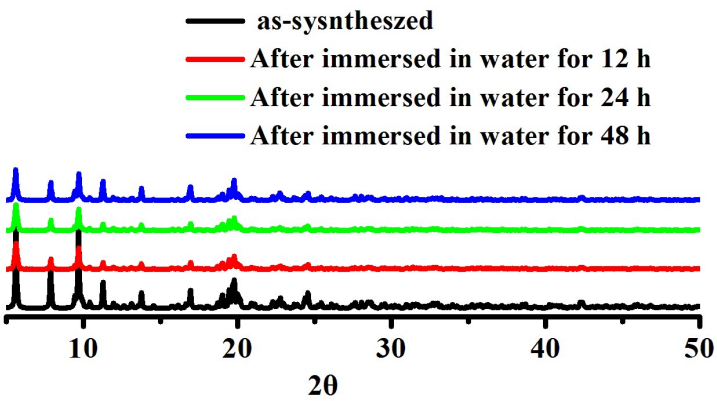

Fig. S4. The chemical stability of Tb-MOF after immersing in water for different time.

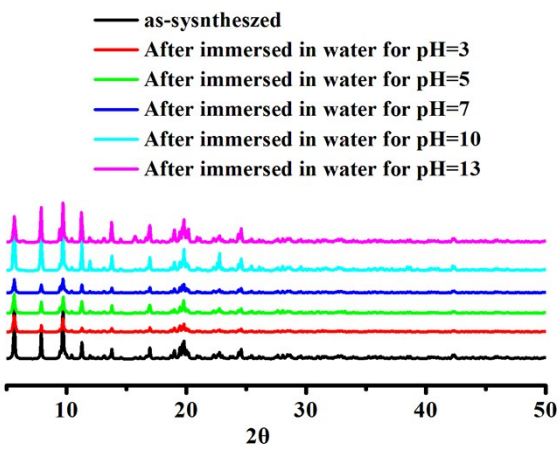

Fig. S5. The chemical stability of Tb-MOF after immersing in water for different pH.

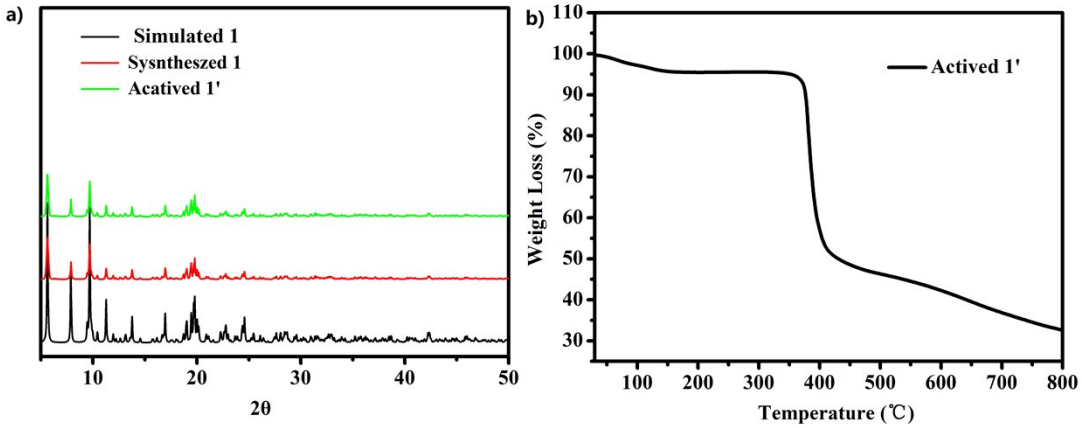

Fig. S6. The curve of PXRD and TG of Tb-MOF'.

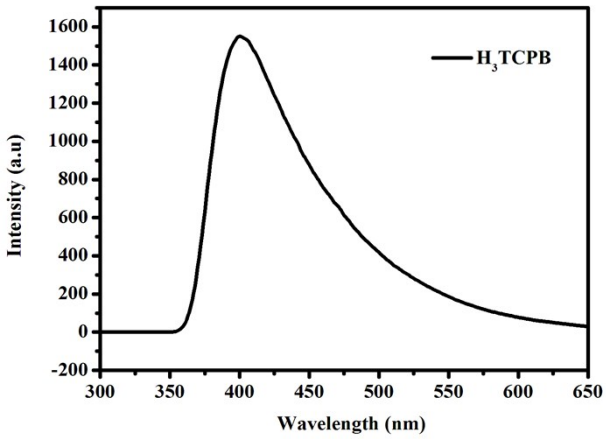

Fig. S7. The solid-state fluorescence spectrum of H_3TCPB ligand.

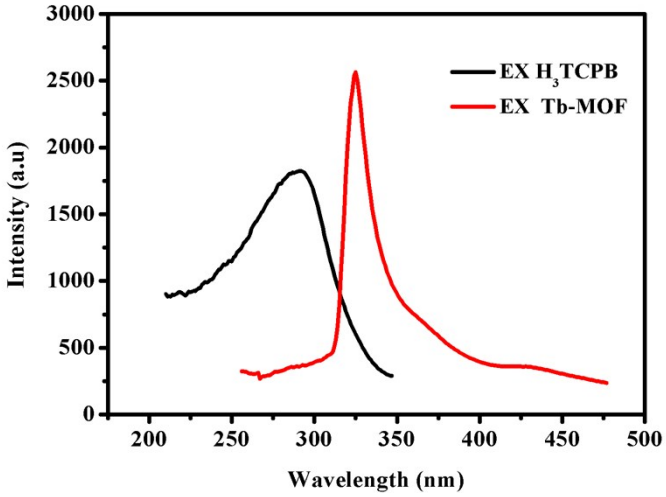

Fig. S8. The exaction spectra of H_3TCPB ligand and Tb-MOF.

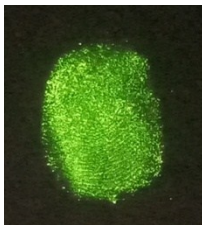

Fig. S9. The optical image of fingerprint under the UV-vis (245nm)

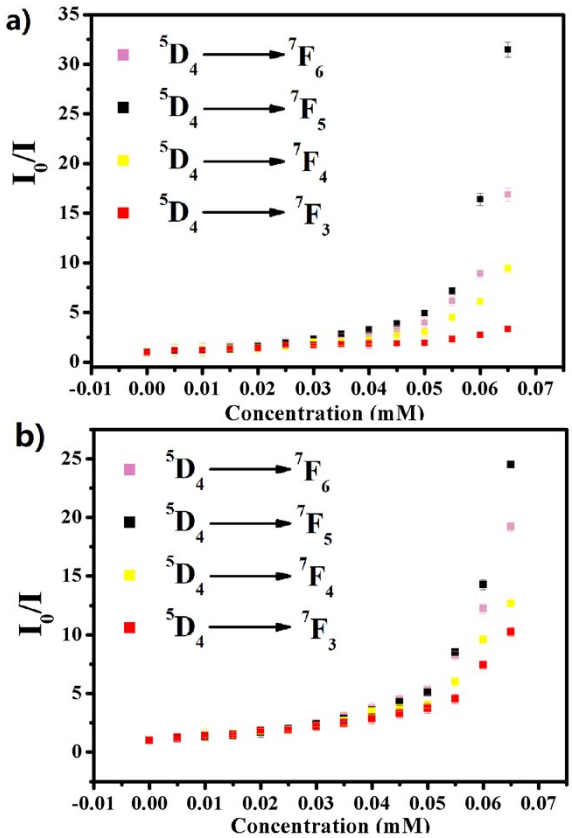

Fig. S10. The relative luminescent intensity (I_0/I) versus the NFT (a) and NZF (b) concentration,

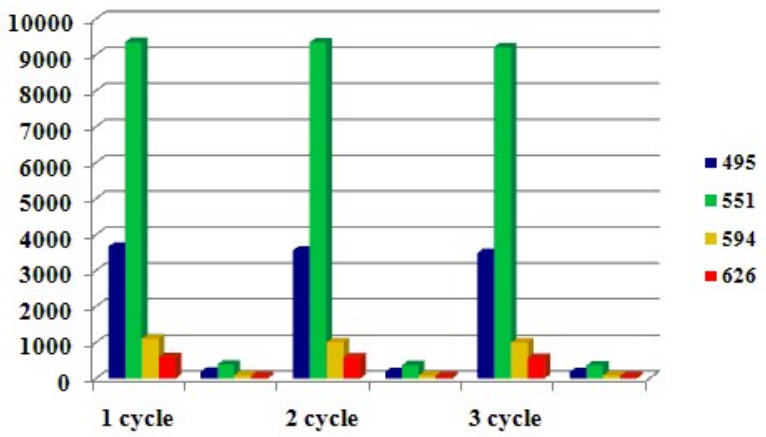

Fig. S11. The results of Tb-MOF for sensing NZF after three continuous cycles.

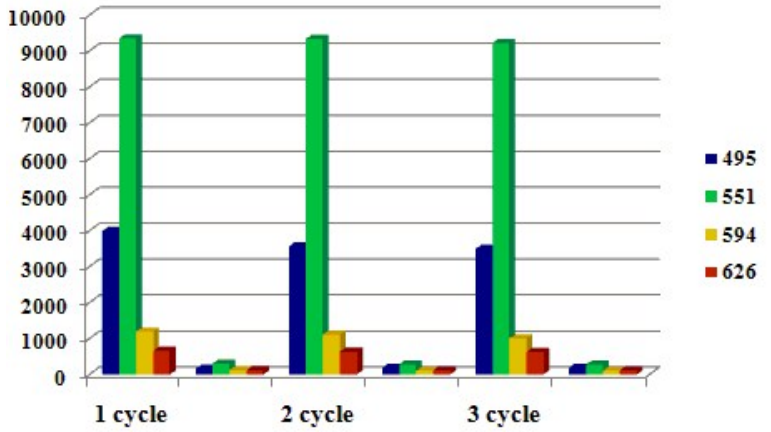

Fig. S12. The results of Tb-MOF for sensing NFT after three continuous cycles.

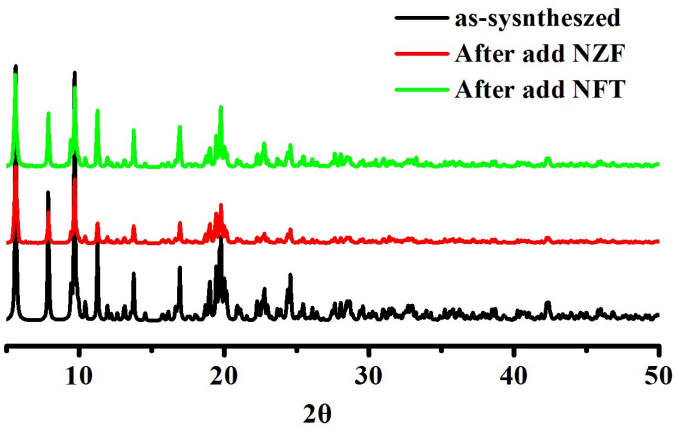

Fig. S13. The PXRD of Tb-MOF after immersing NFs.

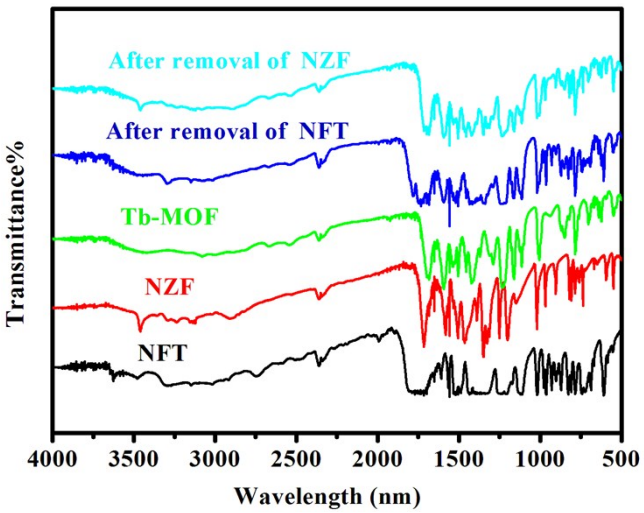

Fig. S14. The IR patterns of pure NZF, NFT, as-synthesized Tb-MOF and the Tb-MOF after immerging in NFT/NZF .

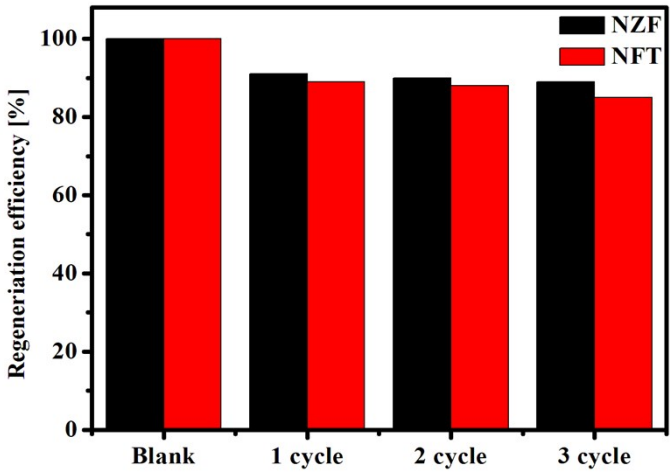

Fig. S15. Regeneration of Tb-MOF for NFT and NZF adsorption.

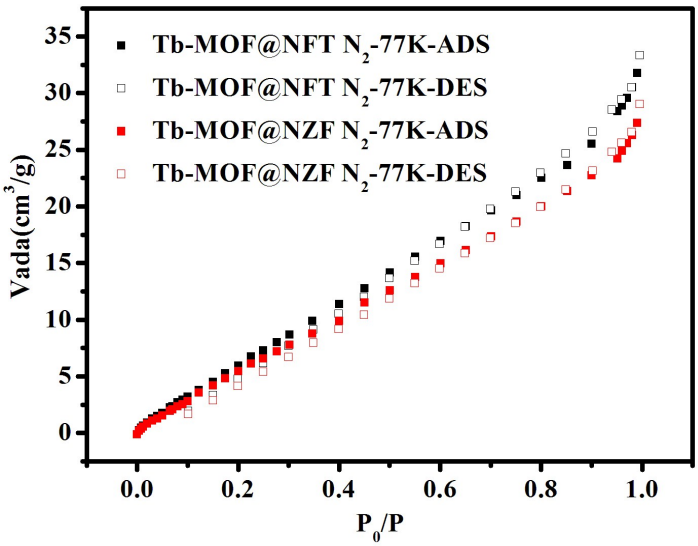

Fig. S16. N_2 adsorption/desorption isotherms of Tb-MOF at 77 K after the removal experiment.